

NuRIA: Numerical Relativity Injection Analysis of signals from generically spinning intermediate mass black hole binaries in Advanced LIGO data

Koustav Chandra,^{1,*} V. Gayathri,^{1,†} Juan Calderón Bustillo,^{2,3,4,‡} and Archana Pai^{1,§}

¹*Department of Physics, Indian Institute of Technology Bombay, Powai, Mumbai, Maharashtra 400076, India*

²*Monash Centre for Astrophysics, School of Physics and Astronomy, Monash University, VIC 3800, Australia*

³*OzGrav: The ARC Centre of Excellence for Gravitational-Wave Discovery, Clayton, VIC 3800, Australia*

⁴*Department of Physics, The Chinese University of Hong Kong, Shatin, N.T., Hong Kong*

The advent of gravitational wave (GW) astronomy has provided us with observations of black holes more massive than those known from X-ray astronomy. However, the observation of an intermediate-mass black hole (IMBH) remains a big challenge. After their second observing run, the LIGO & Virgo Scientific collaborations (LVC) placed upper limits on the coalescence rate density of non-precessing IMBH binaries (IMBHBs). In this Numerical Relativity Injection Analysis (NuRIA), we explore the sensitivity of two of the search pipelines used by the LVC to signals from 69 numerically simulated IMBHBs with total mass greater than $200M_{\odot}$ having generic spins, out of which 27 have a precessing orbital plane. In particular, we compare the matched-filter search PyCBC, and the coherent model-independent search technique cWB. We find that, in general, cWB is more sensitive to IMBHBs than PyCBC, with the difference in sensitivity depending on the masses and spins of the source. Consequently, we use cWB to place the first upper limits on the merger rate of generically spinning IMBH binaries using publicly available data from the first Advanced LIGO observing run.

I. INTRODUCTION

During its first two observing runs (respectively O1 and O2), the gravitational-wave detector network formed by Advanced LIGO [1] and Virgo [2, 3] detected the coalescence of one binary neutron star [4]) and ten binary black holes (BBHs) [4–11]. Also, several independent analyses have reported additional candidates based on their study on publicly available data [12–16].

Since the beginning of the third observing run with much-improved sensitivity, the network has been reporting alerts for astrophysical signals every week, and $\sim \mathcal{O}(100)$ detections are expected by the end of the run. Not only will these observations allow us to study the population and properties of compact binary objects but also lead to the observation of new unobserved sources. For example, the most massive binary neutron star system till date is detected recently in the third observing run [17].

In this Numerical Relativity Injection Analysis (NuRIA), we focus on yet another elusive source: intermediate-mass black holes (IMBHs) [18–23]. These are usually defined as black holes (BHs) with masses in the range of $10^2 - 10^5 M_{\odot}$. They are the missing link between the stellar-mass black holes (SBHs) observed so far by GW detectors (roughly in $18M_{\odot}$ to $85M_{\odot}$ [11]) and the supermassive black holes (SMBHs) with masses larger than $10^5 M_{\odot}$ that are known to lay in the centres of most galaxies. Despite several indirect pieces of evidence for the existence of these objects from electromagnetic

measurements, there is no conclusive direct observation. Such observation would set a milestone for astrophysics, shedding light on how a population of SBHs can transition to SMBHs through, for instance, a hierarchical merger channel [24, 25].

Intermediate mass black hole binaries (IMBHBs) are potentially the loudest sources for current ground-based GW detectors. Despite this, a dedicated search on O1-O2 data reported no detection of any IMBHBs and placed upper limits on their merger rate density [26]. In particular, the most stringent rate upper limit of $0.2 Gpc^{-3} yr^{-1}$ was placed for the case of equal-mass binaries with individual masses $m_1 = m_2 = 100M_{\odot}$ and equal aligned spin parameters of $\chi_{1z} = \chi_{2z} = 0.8$.¹

To place this upper limit, simulated IMBHB signals were injected in the detector data and then recovered with the search algorithms. In [26], for the first time, numerically simulated signals containing all the physics of the IMBHB systems were used, but they were restricted to the systems with BH spins aligned to the orbital plane of the binary. This is a reasonable choice, as the effects of a precessing orbital plane may not be, in principle, observable for short-lived IMBHB signals, vastly dominated by the merger and ringdown emission. However, studies have shown that the effect of precession can be observed in IMBHB systems [27, 28] and hence is interesting to probe the precession effect as detectors become more sensitive to IMBHB systems with an increase in sensitivity.

Hierarchical mergers of BHs in the dense globular clusters are one of the birth-places for IMBHBs. Studies have shown that in such a dense environment, BHs do

* koustav.chandra@iitb.ac.in

† gayathri.v@ligo.org

‡ bustillo@phy.cuhk.edu.hk

§ archana@phy.iitb.ac.in

¹ $\chi_i = \frac{c\mathbf{S}_i}{Gm_i^2}$, with m_i and \mathbf{S}_i being respectively the masses and spins of the two-component objects.

not carry any preferential spin orientation [29]. As a result, binaries formed from these BHs are expected to distribute isotropically in spin orientation resulting in spin-orbit precession.

In this paper, we evaluate the sensitivity of current search algorithms to sources with generic spins and place the first-ever upper limits on their coalescence rate. We use two searches used by the LVC in [26]: the matched-filter algorithm for aligned-spin sources PyCBC [30–32] and the unmodelled time-frequency map-based algorithm, coherent WaveBurst (cWB) [33]. Consistent with a previous work [34], we find cWB is more sensitive than PyCBC to signals from IMBHs, which strongly deviate from the “chirp” which PyCBC targets². Finally, we use cWB to place upper limits on the coalescence rate of a family of IMBHs with generic spins, using publicly available data from the first Advanced LIGO observing run. We place the most constraining upper limit at $0.36/Gpc^3/yr$ on the merger rate density of precessing equal-mass IMBHs with total masses of $210M_\odot$, improving by a factor of ~ 3 on the LVC limits from the O1 run.

The rest of the paper is structured as follows. Section II briefly summarises the impact of precession and higher order-modes on IMBH signals. Section III describes the two search algorithm used in this paper. Section IV describes the analysis setup, including the injections we make in publicly available O1 data [35] and the evaluation of the sensitivity of the searches. In section V, we first compare the sensitivity of the two searches and then report upper limits on a family of IMBHs with generic spins. Finally, in section VI, we summarise our results.

II. SOURCE PROPERTIES AND WAVEFORM MORPHOLOGY

All confirmed gravitational-wave observations of BBHs show a very characteristic chirp morphology. This consists of a monotonically increasing frequency and amplitude during the inspiral and merger stages of the binary, followed by a damped sinusoid with a constant frequency signal during the ringdown. While this is the most extended and studied signal, it is only valid for face-on or nearly face-on BBHs with similar component masses and non-precessing orbital planes. The LIGO BBHs detected so far are consistent with this in terms of their parameters and signal features and henceforth are referred to as *vanilla* BBH.

Generically, the two GR modes of polarisation $h_{+,\times}$ of a GW from a BBH are expressed as a superposition of GW modes $h_{l,m}$ weighted by spin-2 spherical harmonics

($Y_{l,m}^{-2}$) as: [36–38]:

$$h = h_+ - ih_\times = \sum_{l \geq 2} \sum_{m=-l}^{m=l} Y_{l,m}^{-2}(\iota, \Phi) h_{l,m}(\Xi, D_L; t - t_c) \quad (1)$$

where the masses and spins of the individual BHs are collectively denoted by Ξ . The (ι, Φ) are the BBH orientation parameters, D_L is the luminosity distance and t_c denotes the time of coalescence.

For the case of a *vanilla* BBH, the above sum is mostly dominated by the (2, 2) quadrupolar mode which is responsible for the characteristic chirp. However, for asymmetric high-mass sources with orbital plane inclinations away from face-on (i.e., towards $\iota = \pi/2$) configuration, higher modes are significant. This does not only lead to more non-trivial waveform morphologies but can also significantly impact the signal loudness [39–46].

In addition, spin-induced precession introduces amplitude and phase modulations of the individual modes. Spin-precession is triggered by in-plane BH spin components $\chi_{1,2}^\perp$ and the signal amplitude is most impacted by out-of the plane spins $\chi_{1,2}^\parallel$. The effect of the spins in the gravitational waveform is commonly modelled by the *effective-spin precession parameter* χ_p and the *effective-spin parameter* χ_{eff} . These are expressed in terms of the component mass ratio $q = m_1/m_2 \geq 1$ [47–49] as

$$\chi_p = \max\left(\chi_1^\perp, \frac{2 + 3q/2}{q^2} \chi_2^\perp\right), \quad \chi_{eff} = \frac{\chi_1^\parallel m_1 + \chi_2^\parallel m_2}{m_1 + m_2}.$$

Fig. 1 shows that for an asymmetric and nearly edge-on system, an increase in χ_{eff} leads to a longer duration signal and hence louder signal. Also, a non-zero χ_p leads to a significant contribution from higher modes that are resulting in highly non-trivial waveform morphology. Since the PyCBC search implements template that model the dominant (2, 2) mode of aligned-spin sources, we expect it to be inefficient at detecting precessing/asymmetric sources as compared to the unmodelled cWB search.

III. SEARCH ALGORITHM

In this section, we describe the two search algorithms used in NuRIA. The first one, PyCBC, is a matched-filter search that compares the incoming data to waveform templates for the quadrupole mode of aligned-spin BBHs. The second is a model-agnostic search for generic signals coherent across different detectors. Both the algorithms compute the significance of their signal candidates by ranking them together with the accidental background triggers according to a given ranking statistic. To estimate this background, the data of one detector is time-shifted by an amount which falls outside the physically viable time difference of the astrophysically coincident signal [5]. This process, known as time-sliding, is repeated until a sufficient amount of background statistic

² As we will describe later, the PyCBC search is currently restricted to “quadrupole” or $(\ell, m) = (2, \pm 2)$ modes of aligned spin BBHs, omitting higher emission modes.

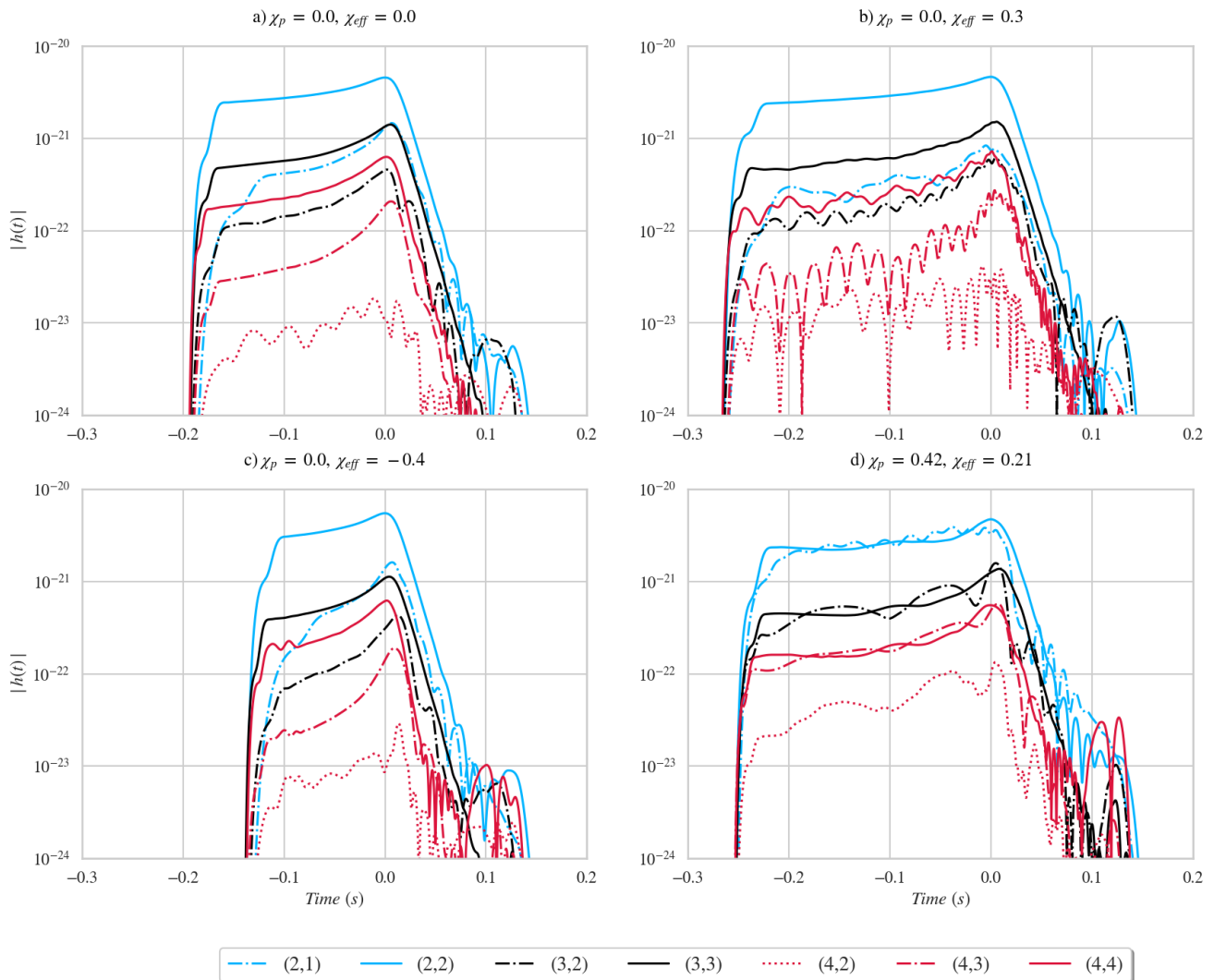


FIG. 1. Amplitude modulus of the gravitational-wave modes of different binary black hole systems with mass ratio $q = 3$ and varying spins and a total mass of $M = 210M_{\odot}$. The systems have edge-on orientation and are located at a distance of 100 Mpc. The source parameters are defined at a starting frequency of 16 Hz. We note that the amplitude of the (3,3) and (4,4) mode increases relative to (2,2) mode from no spin case to systems with spins. The spins also impact both the duration of the signal. The strains have been obtained from the publicly available Georgia Tech catalogue. The corresponding simulations have ID GT0453, GT0596, GT0838 and GT0874. The oscillations in the (4,2) mode in the top left panel are due to numerical noise. We note, however, that the overlap with an equivalent waveform from the SXS code is around 0.94 and the mode itself is so weak that it does not have any significant impact.

is generated. The ranking statistic depends on the actual search and is tailored to provide a clear separation between background triggers and the signals targeted by the search. The final product of these searches is a list of trigger candidates with an associated astrophysical significance which is given by their inverse false alarm rate (IFAR). Triggers above a given IFAR threshold are then recorded as detections.

A. Coherent WaveBurst

Coherent WaveBurst [33] is an unmodelled, multi-detector, all-sky GW transient search based on wavelet transform which looks for excess power in the time-frequency domain. It targets a broad range of generic transient signals, with a minimal assumption about the underlying GW signal. An event is identified by clustering the time-frequency pixels with excess power as compared to the background noise level. Using the constrained maximum likelihood analysis method, the network correlation measures the correlation of the signal between the detectors, and the detection statistics (η_c)

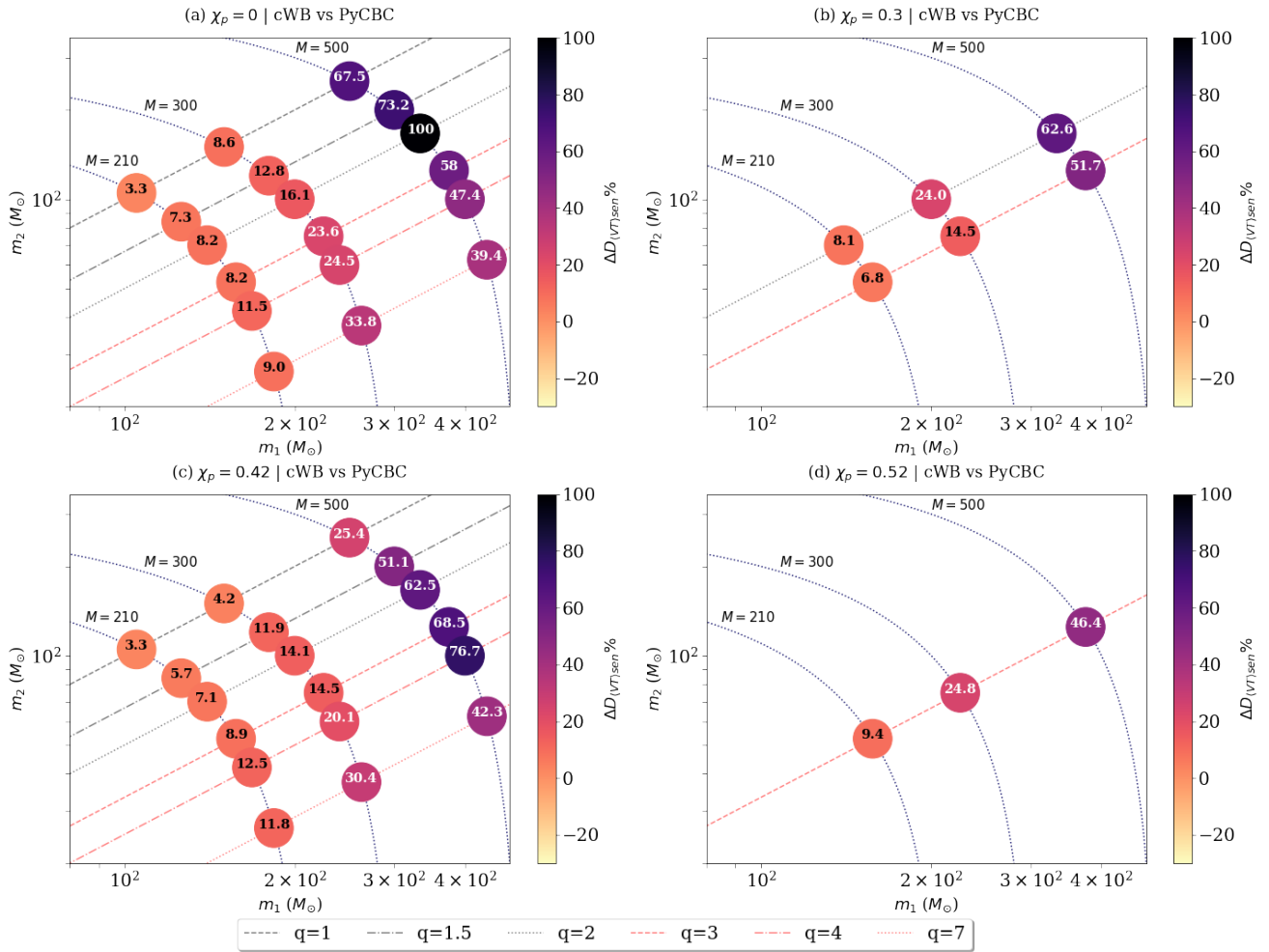


FIG. 2. cWB vs PyCBC: Comparison of the sensitive distance reach of cWB and PyCBC at IFAR=2.94 yr. The results correspond to injections made in the first two chunks of data from the first Advanced LIGO observing run. The effect of higher modes and precession on the search causes the unmodelled algorithm to outperform the matched-filter search as indicated by the positive values.

measures the signal-to-noise ratio. The events are then ranked based on network correlation and η_c , which help to distinguish the real GW from the non-Gaussian noise transients. It uses a large number of noise vetoes to distinguish GW transients from noisy transients (for more details refer to Appendix A in [50]). The noise-based vetoes rely on the residual noise energy per time-frequency pixel per detector and the extent of localisation of the noisy event in the time-frequency plane. Also, the signal based vetoes are developed on the frequency evolution of the signal and the number of wavelets used for a given class of signal reconstruction [51]. The veto values are tuned for IMBHB signals based on simulations study. The cWB ranks candidate events that survived the cWB veto thresholds and are assigned a FAR value given by the rate of the corresponding background events with η_c value more significant than that of the candidate event.

B. The PyCBC search

The PyCBC search matched-filters the incoming detector data d with pre-computed waveform templates h . This filter is optimal when the template is a faithful representation of the GW signal present in the data. The output, known as the signal-to-noise ratio, is given by

$$\rho^2 = 4 \left[\text{Re} \int_{f_{low}}^{f_{high}} \frac{\tilde{d}^*(f) \tilde{h}(f)}{S_n(f)} df \right], \quad (2)$$

where $\tilde{h}(f)$ denotes the Fourier transform of $h(t)$ (For details, [52, 53]). We set minimum and maximum frequencies $f_{low} = 20\text{Hz}$ and $f_{high} = 2048\text{Hz}$, equal to the Nyquist frequency of our data. Coincident triggers across detectors with $\rho > 5.5$ are listed as signal candidate events and signal-template consistency vetoes are applied to these triggers to discriminate real GW signals from noisy transients of terrestrial origin known as

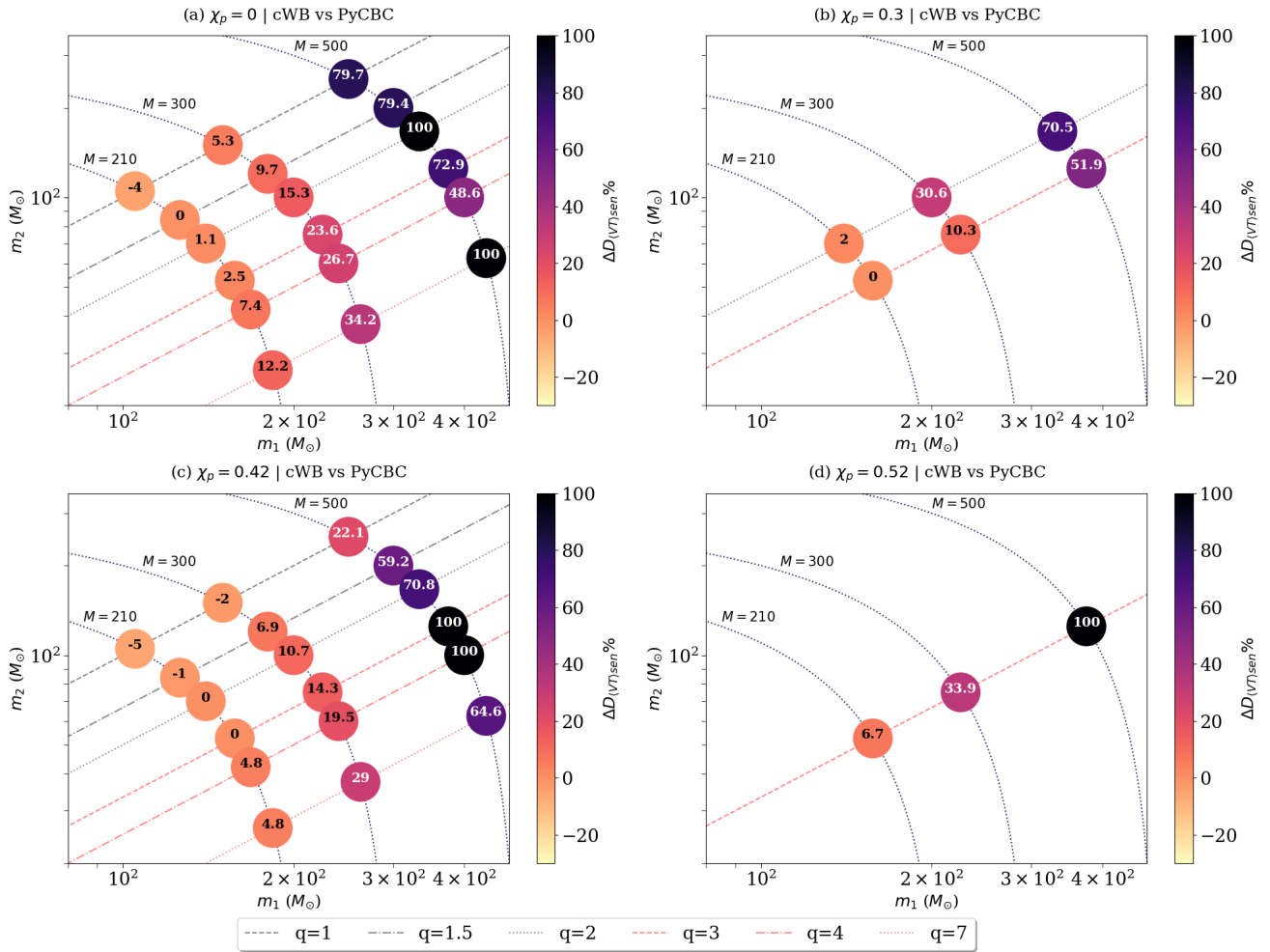


FIG. 3. cWB vs PyCBC: Comparison of sensitive distance reach of cWB and PyCBC, for IFAR=300yr, as a function of the source parameters. The effect of higher modes and precession causes the unmodelled algorithm to outperform (as indicated by positive values) the matched-filter search, which does not incorporate these two effects. We have checked that the apparent alteration of trends at high mass in panels (a) and (c) is consistent with statistical uncertainty.

glitches [54–56]. In particular, the PyCBC search implements a χ^2 signal/glitch discriminator given by [57]

$$\chi_r^2 = \frac{1}{2N-1} \sum_{i=1}^N (\rho_i - \rho_e)^2. \quad (3)$$

Here, ρ_i denotes the SNRs obtained in the i -th frequency band of the detector, chosen so that all of them are expected to produce equal SNR ρ_e if the trigger perfectly matches the template s . If this is the case, then the veto statistic is expected to follow a χ^2 distribution. Therefore, values close to unity are indicative of good signal/template consistency while a mismatch between them will lead to lower or larger values. Finally, the triggers are assigned a ranking statistic [11, 31, 58, 59]

$$\hat{\rho} = \begin{cases} \frac{\rho}{[(1+(\chi_r^2)^n/2)]^{1/n}} & \text{for } \chi_r^2 > 1 \\ \rho & \text{for } \chi_r^2 \leq 1 \end{cases}, \quad (4)$$

which combines ρ and χ_r^2 ³. In addition, we also apply an additional test $\chi_{r,sg}^2$ to deal with instrumental glitches. It determines if the detector output contains any power greater than the maximum expected frequency content of a gravitational wave signal. Using this statistics, we apply a further re-weighting as described in [55] to obtain $\hat{\rho}_{new}$ to obtain single detector triggers. PyCBC then performs a coincidence test on the remaining triggers to obtain candidate events. These candidate events are assigned a ranking statistic which assesses their statistical significance and approximates the likelihood of obtaining the trigger parameters in the presence of a GW signal versus in the case of only noise [60]. The significance of each of this “foreground” trigger is then estimated by comparing its $\hat{\rho}_{new}$ to the background distribution and is usually expressed in terms of inverse FAR in years (yr).

³ Normally $n = 6$

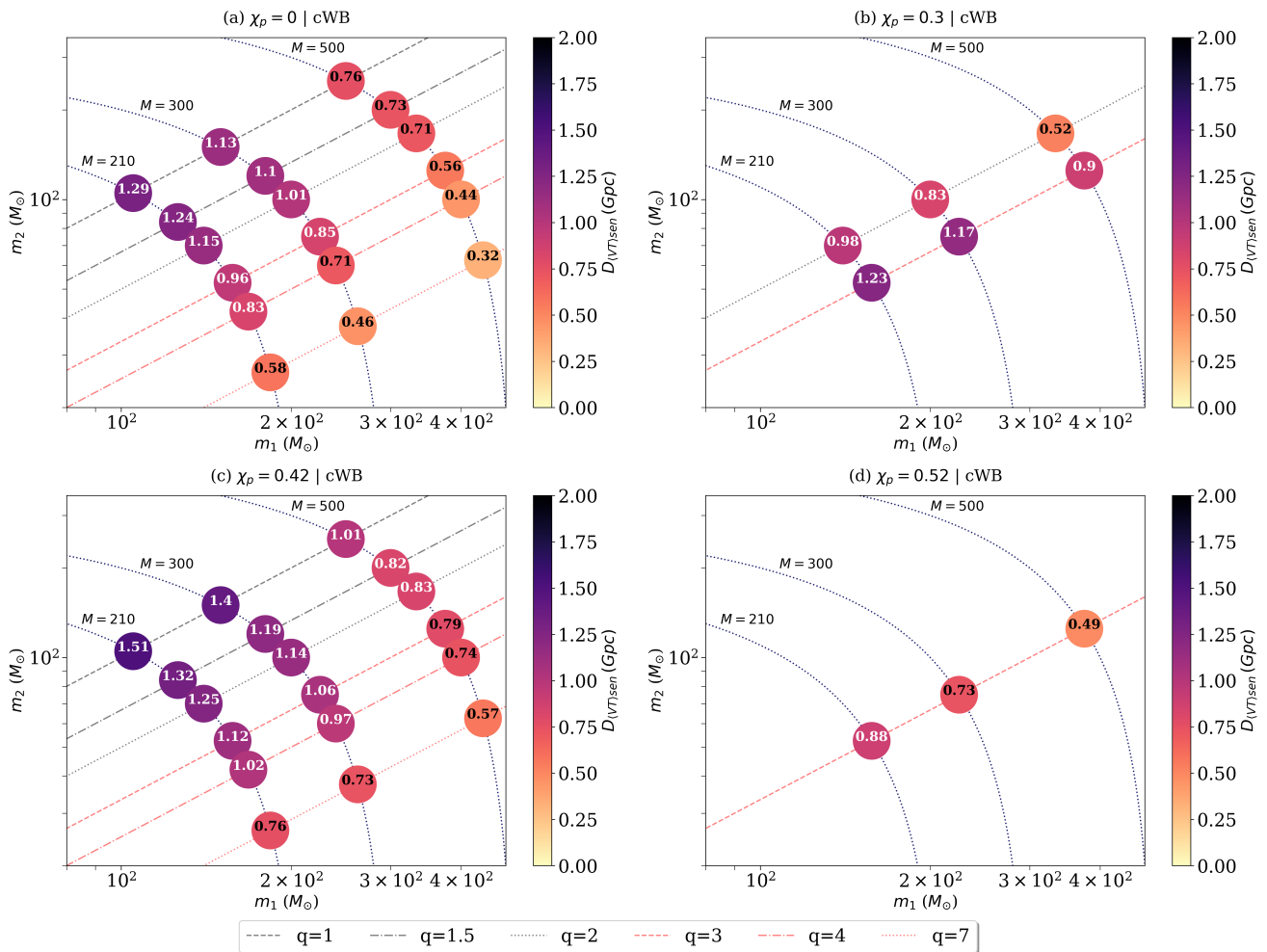


FIG. 4. cWB: The plot shows the sensitive distance reach for this set of injections for IFAR = 2.94yr. As a general trend, the sensitivity drops with increasing total mass and mass ratio.

For this study, we consider the same configuration of PyCBC used for the LIGO-Virgo O1-O2 IMBHB. The template bank [61] targets the $(2, \pm 2)$ modes of BBHs with total masses from $2M_\odot$ to $500M_\odot$, mass ratios up to 98 and restricted to spins aligned (anti-aligned) with the total angular momentum with maximum dimensionless aligned-spin parameter of 0.998. Additionally, the PyCBC algorithm excludes from the template banks templates shorter than $0.15s$ which are more easily mimicked by short glitches [62]. This duration is defined as the time spanned by the template between the minimum frequency of the analysis (20Hz) and its ringdown frequency [61]. As pointed in [61], we argue in Appendix I, this crucially affects the sensitivity of PyCBC at large masses. Finally, templates for BBHs heavier than $4M_\odot$ are computed with the reduced-order effective-one-body model SEOBNRv4ROM [63].

IV. SIMULATION SETUP

A. Injection Set

We inject in the Advanced LIGO O1 data state-of-the-art numerically simulated signals for a large family of IMBHBs with generic spin configurations. Ideally, we would inject an astrophysically motivated population. However, this poses two main caveats. First, the true population of IMBHBs in the Universe is unknown, preventing us from selecting a particular distribution. Second, numerical simulations only cover a discrete set of spins and mass ratios space which prevents the study of a continuous set of sources. We select 27 simulations with given mass ratios and spins, which can be then be scaled to arbitrary masses. These simulations are chosen so that they cover a reasonably wide range of mass ratios, and spin magnitudes and orientations parametrised by the χ_{eff} and χ_p parameters. We scale them to total masses in the range $M = 210M_\odot, 300M_\odot$ and $500M_\odot$.

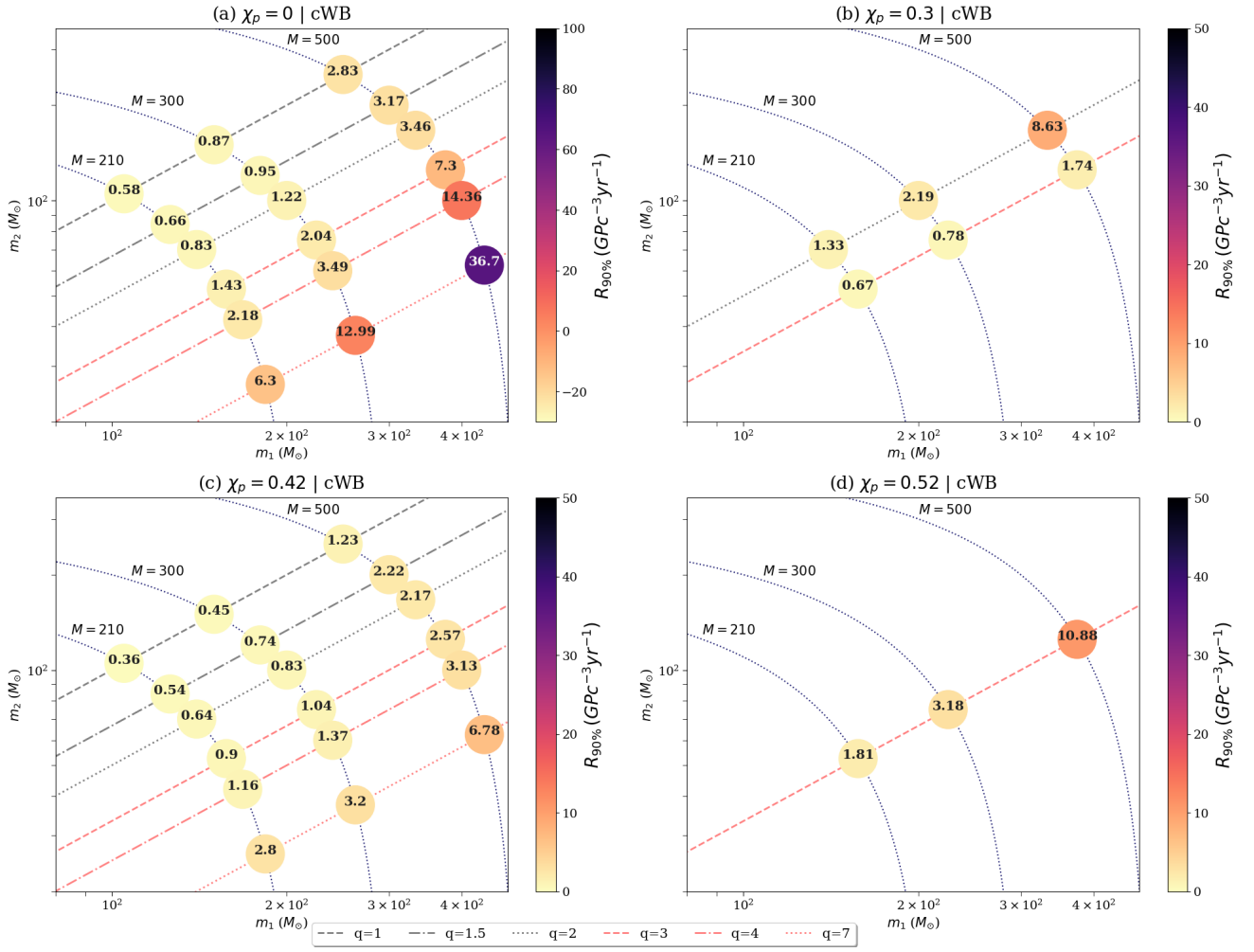


FIG. 5. 90 % upper limit on merger rate density ($R_{90\%}$) for our target IMBHB sources, expressed $Gpc^{-3}yr^{-1}$. We set our most stringent upper limit at $0.36Gpc^{-3}yr^{-1}$ for the symmetric mass system with total mass of $210 M_{\odot}$ and $\chi_p = 0.42$ and $\chi_{eff} = 0.5114$.

Our particular choices are described in Table I. The numerical simulations have been computed by the Georgia Tech group (See Table I for a detailed list) using the Einstein Toolkit code [64, 65] and are publicly available as part of the Georgia Tech Catalogue. The waveforms include the modes = $\{(2, \pm 1), (2, \pm 2), (3, \pm 2), (3 \pm 3), (4, \pm 2), (4, \pm 3), (4, \pm 4)\}$. We do not include further modes as they are usually very weak and dominated by numerical noise.

For each of these, we create injection sets uniformly distributed over the sky sphere, uniformly distributed in the BBH orientation parameters ($\Phi, \cos \iota$), and uniformly distributed in co-moving volume up to a redshift of $z \approx 1$.

B. Sensitive Distance Reach

We determine the sensitivity of a search to each of our sources by calculating the corresponding sensitive distance reach. To do that, we inject a set of N_{tot} in-

jections distributed uniformly over the comoving volume $VT_{tot}[Gpc^3yr]$ into O1 data and recover them using our search algorithms. We consider as detections those recovered with significance equal or larger than a predetermined threshold [66, 67]. Denoting by N_{rec} the number of detected injections, the corresponding sensitive volume and reach are computed as

$$\langle VT \rangle_{sen} = \frac{N_{rec}}{N_{tot}} \langle VT \rangle_{tot}, \quad (5)$$

$$D_{\langle VT \rangle_{sen}} = \left[\frac{3 \langle VT \rangle_{sen}}{4\pi T_a} \right]^{1/3}, \quad (6)$$

where T_a is the total analysis time [26]. To compare the sensitivity of the two pipelines to the IMBH sources, we compute the fractional difference in sensitive distance



FIG. 6. Sensitivity of cWB as a function of the binary spins. When $\chi_p = 0$, an increase in χ_{eff} , causes an increment of the sensitive distance reach while a decrease in χ_{eff} causes the sensitivity to drop.

reach in percentage as

$$\Delta D_{\langle VT \rangle_{sen}} [\%] = \left(\frac{D_{\langle VT \rangle_{sen}}^{cWB} - D_{\langle VT \rangle_{sen}}^{PyCBC}}{D_{\langle VT \rangle_{sen}}^{cWB}} \right) \times 100. \quad (7)$$

The positive values indicate better performance of cWB compared to PyCBC and vice-a-versa. We note that the statistical uncertainty in N_{rec} is $\sigma(N_{rec}) = 1/\sqrt{N_{rec}}$. Since cWB will be reasonably sensitive to all of our injection sets, we find that the corresponding sensitive

distance uncertainties range in 4 – 7%. However, for PyCBC the number of recovered injections can be as low as zero for the largest masses and mass ratios. For these cases, we will consider that a suitable statistical noise fluctuation would yield, at most, 1 recovered injection, giving an uncertainty of 100%.

Finally, for a given search, we place an astrophysical upper limit on the merger rate density at the 90 % con-

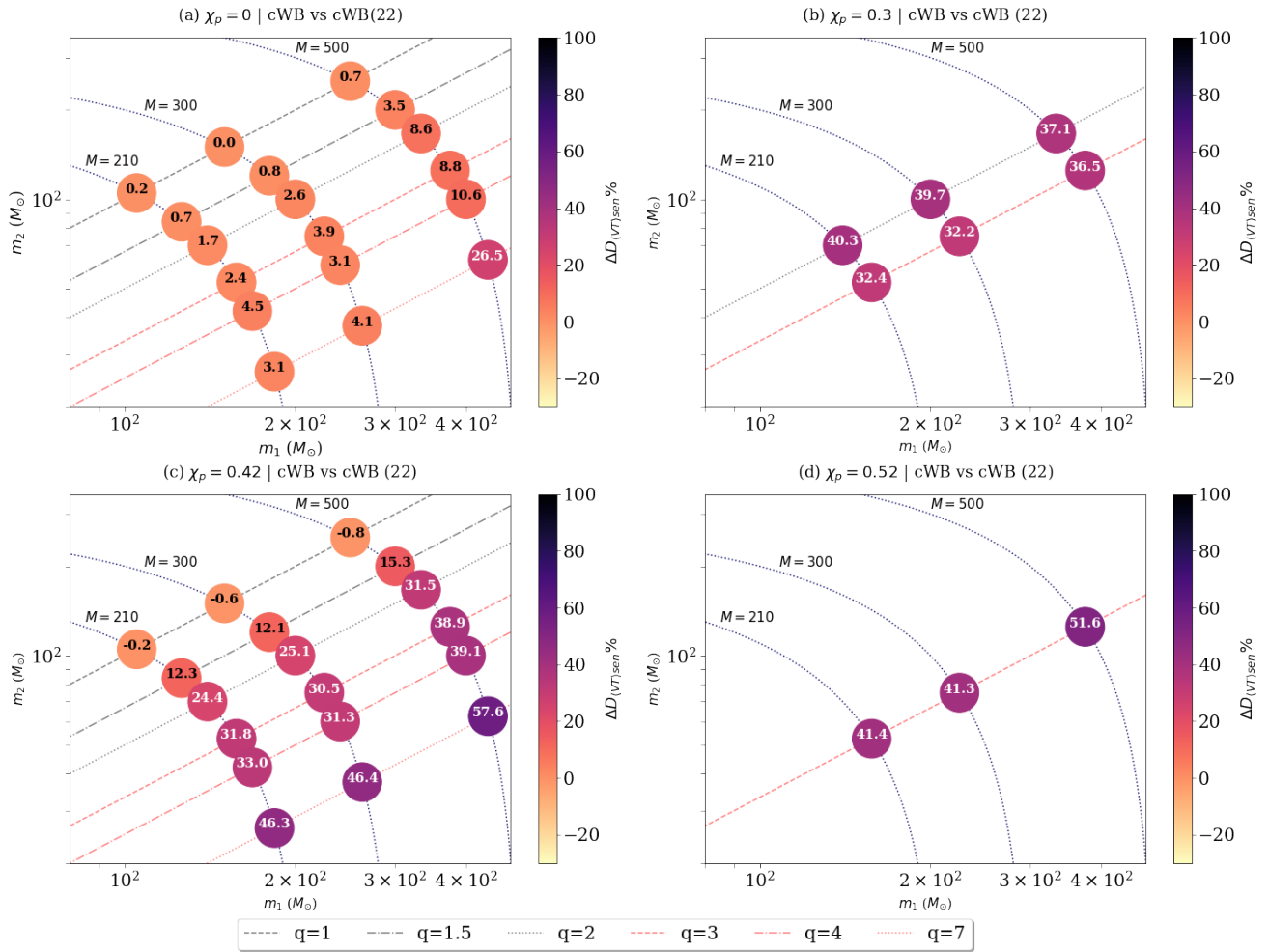


FIG. 7. Ratio of the sensitivity of cWB to signals including and omitting higher modes. Values of Δ_D indicate that cWB is equally sensitive to both kinds of signals while large values indicate an increase in the sensitivity when higher modes are included. The higher modes provide extra signal power as the total mass and mass ratio increase, leading to an important increment of the sensitivity of the search.

fidence level as obtained by [26, 68]:

$$R_{90\%} = -\frac{\ln 0.1}{\langle VT \rangle_{sen}}. \quad (8)$$

V. RESULTS

In this section, we first compare the sensitivity of the two search algorithms using a fraction of O1 data (between September 12 - October 8, 2015) and find that cWB largely over-performs PyCBC in most cases. Next, we place upper limits on the coalescence rate density for a precessing set using O1 data using the results of the cWB search.

A. Comparing the searches

We compare the sensitivity of our searches at two reference significance thresholds given by IFARs of 2.94yr⁴ and 300yr. At low IFAR, the significance of the PyCBC triggers is mostly given by the recovered SNR so that a good separation of injections from the background is not required. Hence, subtle physical effects that cause a signal-template mismatch may not play a role in the search comparison.

At a larger IFAR of 300yr, the worsening effect comes because of mismatch between the signals and the quadrupolar templates and hence large deviations of χ^2 from unity. Fig. 2 shows $\Delta D_{(VT)_{sen}}$, at an IFAR threshold of 2.94yr, for all the sources considered in this study,

⁴ This is motivated by loudest IMBH-like trigger reported in [26]

χ_p	χ_{eff}	q	SIM ID
0	-0.6	2, 3	GT0837,GT0846
	-0.4	1, 1.5, 2	GT0564,GT0836,GT0838
		3	GT0841
	0	1,1.5,2	GT0905,GT0477,GT0446
	0	3,4,7	GT0453,GT0454, GT0818
	0.4	1,1.5,2	GT0422,GT0558,GT0472
0.3	0.3	3	GT0596
	0.4, 0.45	2, 3	GT0588,GT0600
	-0.35	2	GT0437
0.42	0.52	3	GT0732
	0.51, 0.09	1,1.5	GT0803,GT0873
	0.14, 0.21	2,3	GT0872, GT0874
0.52	0.25, 0.32	4,7	GT0875,GT0888
	-0.3	3	GT0729
0.6	0	3	GT0696

TABLE I. Summary of Georgia Tech NR simulations used to model our target signals. The source parameters are defined at the starting frequency of 16 Hz.

expressed in the (m_1, m_2) plane, with varying χ_p and χ_{eff} . For most cases, cWB out-performs PyCBC, so that $\Delta D_{(VT)_{sen}} > 0$. In agreement with previous studies restricted to aligned-spins [26], the difference between the two searches increases with an increase in total mass for fixed mass-ratio and spin parameters. This is partially due to the increasing contribution of higher-modes to the signals, not included in the PyCBC search templates. On the one hand, the mismatch between injections and templates leads to a poor SNR recovery. (For details check [34]). On the other, it increases the χ_r^2 statistic, making the search interpret the injections as glitches. Additionally, we note that even in the absence of higher-modes, it has been shown in the past that the χ_r^2 discriminator performs poorly at separating short-duration signals from glitches [55, 69].

We note that, in a somewhat unexpected way, for bin $(M = 500M_\odot, q = 2)$ PyCBC was not able to recover any injection while some injections are recovered for the neighbouring $q = 1.5$ and $q = 3$ cases. We attribute this to a combination of the large statistical uncertainty of the PyCBC sensitive range and the physical properties of the sources. First, the very low number of recovered injections $N_{rec} \in [1, 5]$ at such large masses yields relatively large uncertainties $\sigma(N_{rec}) = 1/\sqrt{N_{rec}}$. Second, at such large masses, the $(2, 2)$ mode of the system can be mostly out of the sensitive band so that the PyCBC templates can effectively match the next mode remaining in the band, namely the $(3, 3)$ instead of having to match a combination of modes. Such modes are more prominent for increasing mass ratio. Finally, note that performance of PyCBC relative to cWB improves for larger mass ratios due the decreasing sensitivity of cWB, shown in Fig.4(a). A similar effect is also noticeable in Fig. 2(c). A detailed description about the physical reason for missing the mass-bin is given in Appendix A.

At a larger IFAR, mismatches between injections and templates affect the sensitivity of PyCBC. As a conse-

quence, there is a reduction in its sensitivity toward high total mass and high mass ratio sources with more considerable higher mode contribution. Consistently, even at this IFAR (see Fig. (3)) we find that the two pipelines have a comparable performance for low mass and low mass ratio systems, as the impact of precession / higher modes on the signals being less important in these cases.

We conclude that, as expected, the signal morphology of IMBHB sources – *short signals with potentially complex morphology in the case of edge-on, large mass ratio cases* – is better captured by the model agnostic cWB search than the by the PyCBC search. In the following, we report the simulation results with cWB using the entire duration of O1.

B. IMBHBs with generic spins

We estimate the sensitive distance reach using Eq.6. As a general trend, we observe that the sensitivity decreases with increasing total mass and mass-ratio. This is expected as the duration of signal shortens in the detector band, the loudness of the signal decreases. As mentioned before, a positive χ_{eff} leads to a longer signal. For this reason, in Fig. 4 (b), we observe a larger sensitive volume for $q = 3$, than for the $q = 2$ case, which has negative χ_{eff} . For this same reason, the cases with $(\chi_p, \chi_{eff}) = (0.4)$ and positive χ_{eff} in Fig. 3(c) shows the largest distance reach among all sources.

We compute the corresponding 90% merger rate density using eq. (8). These are shown in Fig. 5. We place the most constraining upper limit of $0.36/Gpc^3/yr$ on the merger rate of equal-mass IMBHs with $M = 210M_\odot$ and effective spin parameters $(\chi_p, \chi_{eff}) = (0.4, 0.51)$. We note this upper limit improves by a factor of ~ 3 on the one obtained for aligned-spin sources after the first Advanced LIGO observing run [70]. This is less constraining than the one obtained after the second run before which the detectors underwent major up-gradation to obtain better sensitivity. Better sensitivity shows that generically spinning sources may offer a better chance to observe BBHs in this mass range.

C. Precession vs. aligned spins

It is natural to ask if the effects of precession and aligned-spins, parametrised respectively by χ_p and χ_{eff} , can be somewhat disentangled in terms of the sensitivity. To do this, we compute the sensitivity to sources with fixed mass-ratio and total mass; with $\chi_p = 0$ and varying χ_{eff} , and varying χ_p for fixed χ_{eff} . The right panels of Fig. 6 show the results for the case of $q = 3$. As expected, for fixed $\chi_p = 0$, a positive (negative) χ_{eff} leads to larger (lower) sensitive distance reach. Besides, we observe that a variation of χ_p produces a variation between 4% to 7% in the sensitive range for a fixed χ_{eff} . Similar results are observed for the $q = 2$ cases shown in

the left panels. Given this, we conclude that for these mass ratios, the sensitive distance reach is not significantly affected by the value of χ_p .

D. Impact of higher-order modes

Finally, similar to what was done in [34] for aligned-spin sources, we look at the impact of the inclusion/omission of the higher modes. To this, we compare the sensitivity of our search to injection sets including and omitting this effect. Fig.7 shows the fractional increase of sensitive distance produced by the inclusion of higher-order modes in our injections. We observe that the sensitivity of the pipeline increases when the higher-modes are included in the injections, as this generally increases the available signal power. Since higher-modes have a larger impact on the case of large mass-ratio and large total-mass sources, the impact in the sensitive distance reach is larger in these cases. An increment as large as $\sim 57\%$ is observed for the system with $\chi_p = 0.42$, $M = 500M_\odot$ and $q = 7$. An apparent deviation from this rule can be observed in panel b, in which the impact of HMs is larger for the $q = 2$ than for the $q = 3$ case. The reason is that while the $q = 3$ case has a $\chi_{eff} > 0$ that makes the signal long in the detector sensitive band, the $q = 2$ case has $\chi_{eff} < 0$. The latter leads to a short observable signal more dominated by its merger and ringdown portions, in which HMs are more prominent. Finally, we note that negative values apparently indicating that a larger sensitivity is obtained when HMs are omitted, are statistically consistent with zero.

VI. CONCLUSION

The detection of intermediate-mass black holes is a standing challenge in astronomy. Despite being one of the loudest sources for advanced gravitational-wave detectors, the shorter duration of the signals in the detector sensitive band and the prominent impact of higher modes and possibly precession (not captured by model-based searches) makes their detection more difficult than that of lighter binary black holes. In this situation, unmodelled searches have shown to be a promising method toward the detection of such objects [26]. In NuRIA, for the first time, we present a comprehensive study on the ability of current gravitational-wave searches to detect generic spinning IMBHs. We focus on two searches used by the LIGO-Virgo collaborations in their recent second observing runs: the matched-filter algorithm PyCBC and model agnostic cWB. We find that at their present status, the latter offers a much better prospect to observe IMBHs in GW window. Finally, we have placed the first-ever upper limits on the coalescence rate of precessing IMBHs using data from the first Advanced LIGO observing run using the un-modelled search. We place our most stringent 90% coalescence rate density

upper limit of $0.36/Gpc^3/yr$ for equal mass and precessing system with a total mass of $210M_\odot$. This improves on the $0.94/Gpc^3/yr$ placed for aligned-spin IMBHs after the first Advanced LIGO observing run. The higher sensitive distance reach of precessing systems indicate that generically spinning sources offer a better chance for the detection of BBHs in this mass range. While the upper limit on rate density has been pushed to $0.2/Gpc^3/yr$ after the second observing run, we expect that more constraining limits when these are computed using injections from generically spinning binaries as well as when the detectors become more and more sensitive.

VII. ACKNOWLEDGEMENTS

The authors thank Grace Kim for sharing with us a detailed comparison between Georgia Tech and SXS waveforms. The authors are grateful for the computational resources provided by the LIGO Laboratory and supported by National Science Foundation Grants PHY-0757058 and PHY-0823459. This research has made use of data obtained from the Gravitational Wave Open Science Center (<https://www.gwopenscience.org>) [35], a service of LIGO Laboratory, the LIGO Scientific Collaboration and the Virgo Collaboration. We also thank the LIGO-VIRGO IMBHB group, the PyCBC and the cWB team for their help and support, especially Sebastian Khan, Ian Harry, Sergey Klimentko, Imre Bartos, Leslie Wade and Thomas Dent. KC acknowledges the MHRD, Government of India for the fellowship support. VG recognises Inspire division, Department of Science and Technology, Government of India for the fellowship support. J.C.B is supported by the Australian Research Council Discovery Project DP180103155 and by the Direct Grant, Project 4053406, from the Research Committee of the Chinese University of Hong Kong. AP thanks the IRCC, SEED grant, IIT Bombay for the support. This document has LIGO DCC number P1900366.

Appendix A: Investigating PyCBC's poor performance at high masses

In this appendix we provide visual intuition on the poor performance of PyCBC for large masses. The top panel of Fig. 8, shows the spectrum of the (2,2) and (3,3) modes of the non-spinning $q = 2$ simulation GT0446, scaled to $500M_\odot$, for which PyCBC could not recover any injection. The bottom panel, shows the frequency and amplitude of the dominant (2,2) as a function of time. We note that oscillations in the frequency become more pronounced as the signal becomes weaker and the simulation is dominated by numerical noise.

First, the top panel shows that even though the (3,3) mode spans a larger range of frequencies above the Ad-

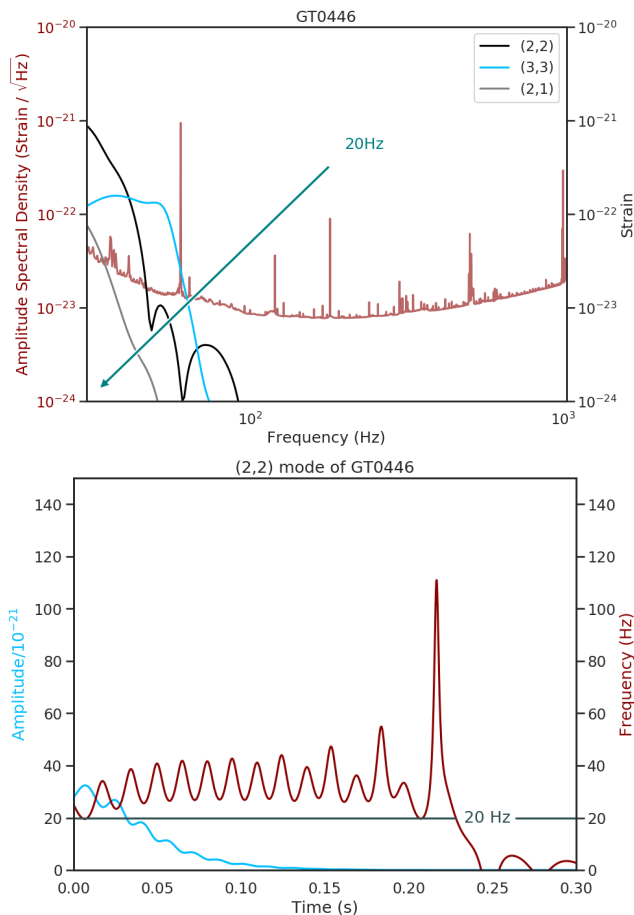


FIG. 8. Top: Amplitude of the Fourier transforms of the (2, 2) and (3, 3) modes of the GT0446 numerical simulation scaled to total mass of $500M_{\odot}$ at a distance of 100Mpc. We have chosen an inclination $\iota = 60^{\circ}$ to make the (3, 3) mode sufficiently prominent. Bottom: Frequency and amplitude of the (2, 2) as a function of time.

vanced LIGO noise, the (2, 2) mode is an order of magnitude stronger, so the presence of higher modes does not seem to be the cause of PyCBC’s poor performance. However, the bottom panel shows that the time spanned by the (2, 2) after reaching 20Hz is below the minimum threshold of 0.15s template duration imposed by the PyCBC template bank [61]. Moreover, we note that while this threshold refers to the time spanned by the template between 20Hz and its ringdown frequency, the duration of the *full waveform* within the analysis frequency band is actually shorter than 0.15s. Consequently, even if a putative template including only the (2, 2)-mode could recover the signal, this would be automatically discarded by PyCBC. While PyCBC uses this strategy to avoid the accumulation of large amount of triggers caused by short glitches [62], this decreases the ability of the template-bank based matched-filter search to recover IMBHB signals.

-
- [1] J. Aasi *et al.* (LIGO Scientific), *Class. Quant. Grav.* **32**, 074001 (2015), [arXiv:1411.4547 \[gr-qc\]](#).
- [2] F. Acernese *et al.* (VIRGO), *Class. Quant. Grav.* **32**, 024001 (2015), [arXiv:1408.3978 \[gr-qc\]](#).
- [3] F. Acernese *et al.* (Virgo), *Class. Quant. Grav.* **35**, 205004 (2018), [arXiv:1807.03275 \[gr-qc\]](#).
- [4] B. Abbott *et al.* (LIGO Scientific Collaboration, Virgo Collaboration), *Phys. Rev. Lett.* **119**, 161101 (2017), [arXiv:1710.05832 \[gr-qc\]](#).
- [5] B. P. Abbott *et al.* (LIGO Scientific Collaboration, Virgo Collaboration), *Phys. Rev. Lett.* **116**, 061102 (2016), [arXiv:1602.03837 \[gr-qc\]](#).
- [6] B. P. Abbott *et al.* (LIGO Scientific Collaboration, Virgo Collaboration), *Phys. Rev. Lett.* **116**, 241103 (2016), [arXiv:1606.04855 \[gr-qc\]](#).
- [7] B. P. Abbott *et al.* (LIGO Scientific Collaboration, Virgo Collaboration), *Phys. Rev. Lett.* **118**, 221101 (2017), [arXiv:1706.01812 \[gr-qc\]](#).
- [8] B. P. Abbott *et al.* (LIGO Scientific Collaboration, Virgo Collaboration), *Astrophys. J.* **851**, L35 (2017), [arXiv:1711.05578 \[astro-ph.HE\]](#).
- [9] B. P. Abbott *et al.* (LIGO Scientific Collaboration, Virgo Collaboration), *Phys. Rev. Lett.* **119**, 141101 (2017), [arXiv:1709.09660 \[gr-qc\]](#).
- [10] B. P. Abbott *et al.* (LIGO Scientific Collaboration, Virgo Collaboration), *Phys. Rev.* **X6**, 041015 (2016), [erratum: *Phys. Rev.* X8, no.3, 039903(2018)], [arXiv:1606.04856 \[gr-qc\]](#).
- [11] B. P. Abbott *et al.* (LIGO Scientific, Virgo), *Phys. Rev.* **X9**, 031040 (2019), [arXiv:1811.12907 \[astro-ph.HE\]](#).
- [12] A. H. Nitz, C. Capano, A. B. Nielsen, S. Reyes, R. White, D. A. Brown, and B. Krishnan, *Astrophys. J.* **872**, 195 (2019), [arXiv:1811.01921 \[gr-qc\]](#).
- [13] A. H. Nitz, T. Dent, G. S. Davies, S. Kumar, C. D. Capano, I. Harry, S. Mozzon, L. Nuttall, A. Lundgren, and M. Tpai, *Astrophys. J.* **891**, 123 (2019), [arXiv:1910.05331 \[astro-ph.HE\]](#).
- [14] T. Venumadhav, B. Zackay, J. Roulet, L. Dai, and

- M. Zaldarriaga, *Phys. Rev.* **D100**, 023011 (2019), [arXiv:1902.10341 \[astro-ph.IM\]](#).
- [15] T. Venumadhav, B. Zackay, J. Roulet, L. Dai, and M. Zaldarriaga, (2019), [arXiv:1904.07214 \[astro-ph.HE\]](#).
- [16] J. M. Antelis and C. Moreno, *Gen. Rel. Grav.* **51**, 61 (2019), [arXiv:1807.07660 \[gr-qc\]](#).
- [17] B. P. Abbott *et al.* (LIGO Scientific, Virgo), *Astrophys. J. Lett.* **892**, L3 (2020), [arXiv:2001.01761 \[astro-ph.HE\]](#).
- [18] D. M. Eardley and W. H. Press, *Annual Review of Astronomy and Astrophysics* **13**, 381 (1975), <https://doi.org/10.1146/annurev.aa.13.090175.002121>.
- [19] M. J. Rees, *The Observatory* **98**, 210 (1978).
- [20] J. N. Bahcall and J. P. Ostriker, *Nature (London)* **256**, 23 (1975).
- [21] M. C. Begelman and M. J. Rees, *mnras* **185**, 847 (1978).
- [22] G. D. Quinlan and S. L. Shapiro, *Astrophys. J.* **356**, 483 (1990).
- [23] J. E. Greene, J. Strader, and L. C. Ho, (2019), [arXiv:1911.09678 \[astro-ph.GA\]](#).
- [24] M. Mezcua, *International Journal of Modern Physics D* **26**, 1730021 (2017), [arXiv:1705.09667](#).
- [25] F. Koliopoulos, in *Proceedings of the XII Multifrequency Behaviour of High Energy Cosmic Sources Workshop. 12-17 June* (2017) p. 51, [arXiv:1801.01095 \[astro-ph.GA\]](#).
- [26] B. P. Abbott *et al.* (LIGO Scientific, Virgo), *Phys. Rev.* **D100**, 064064 (2019), [arXiv:1906.08000 \[gr-qc\]](#).
- [27] M. Mapelli, *Mon. Not. Roy. Astron. Soc.* **459**, 3432 (2016), [arXiv:1604.03559 \[astro-ph.GA\]](#).
- [28] J. Calderon Bustillo, N. Sanchis-Gual, A. Torres-Forné, and J. A. Font, In prep. (2019).
- [29] C. L. Rodriguez, S. Chatterjee, and F. A. Rasio, *Phys. Rev.* **D93**, 084029 (2016), [arXiv:1602.02444 \[astro-ph.HE\]](#).
- [30] T. Dal Canton *et al.*, *Phys. Rev.* **D90**, 082004 (2014), [arXiv:1405.6731 \[gr-qc\]](#).
- [31] S. A. Usman *et al.*, *Class. Quant. Grav.* **33**, 215004 (2016), [arXiv:1508.02357 \[gr-qc\]](#).
- [32] A. H. Nitz, I. W. Harry, J. L. Willis, C. M. Biwer, D. A. Brown, L. P. Pekowsky, T. Dal Canton, A. R. Williamson, T. Dent, C. D. Capano, T. J. Massinger, A. K. Lenon, A. B. Nielsen, and M. Cabero, “PyCBC Software,” github.com/ligo-cbc/pycbc (2017).
- [33] S. Klimenko *et al.*, *Phys. Rev.* **D93**, 042004 (2016), [arXiv:1511.05999 \[gr-qc\]](#).
- [34] J. Calderón Bustillo, P. Laguna, and D. Shoemaker, *Phys. Rev. D* **95**, 104038 (2017).
- [35] R. Abbott *et al.* (LIGO Scientific, Virgo), (2019), [arXiv:1912.11716 \[gr-qc\]](#).
- [36] J. N. Goldberg, A. J. MacFarlane, E. T. Newman, F. Rohrlich, and E. C. G. Sudarshan, *J. Math. Phys.* **8**, 2155 (1967).
- [37] M. Maggiore, *Gravitational Waves: Volume 1: Theory and Experiments*, Gravitational Waves (OUP Oxford, 2008).
- [38] J. Creighton and W. Anderson, *Gravitational-Wave Physics and Astronomy: An Introduction to Theory, Experiment and Data Analysis*, Wiley Series in Cosmology (Wiley, 2012).
- [39] L. Pekowsky, J. Healy, D. Shoemaker, and P. Laguna, *Phys. Rev.* **D87**, 084008 (2013), [arXiv:1210.1891 \[gr-qc\]](#).
- [40] V. Varma, P. Ajith, S. Husa, J. C. Bustillo, M. Hannam, and M. Pürrer, *Phys. Rev.* **D90**, 124004 (2014), [arXiv:1409.2349 \[gr-qc\]](#).
- [41] J. Calderón Bustillo, S. Husa, A. M. Sintes, and M. Pürrer, *Phys. Rev.* **D93**, 084019 (2016), [arXiv:1511.02060 \[gr-qc\]](#).
- [42] V. Varma and P. Ajith, *Phys. Rev. D* **96**, 124024 (2017).
- [43] J. Calderón Bustillo, P. Laguna, and D. Shoemaker, *Phys. Rev.* **D95**, 104038 (2017), [arXiv:1612.02340 \[gr-qc\]](#).
- [44] P. B. Graff, A. Buonanno, and B. Sathyaprakash, *Phys. Rev.* **D92**, 022002 (2015), [arXiv:1504.04766 \[gr-qc\]](#).
- [45] J. Calderón Bustillo, J. A. Clark, P. Laguna, and D. Shoemaker, *Phys. Rev. Lett.* **121**, 191102 (2018), [arXiv:1806.11160 \[gr-qc\]](#).
- [46] J. Calderón Bustillo, C. Evans, J. A. Clark, G. Kim, P. Laguna, and D. Shoemaker, *arXiv e-prints*, [arXiv:1906.01153 \(2019\)](#), [arXiv:1906.01153 \[gr-qc\]](#).
- [47] E. Poisson and C. M. Will, *Phys. Rev. D* **52**, 848 (1995).
- [48] L. Santamaria *et al.*, *Phys. Rev.* **D82**, 064016 (2010), [arXiv:1005.3306 \[gr-qc\]](#).
- [49] P. Schmidt, F. Ohme, and M. Hannam, *Phys. Rev.* **D91**, 024043 (2015), [arXiv:1408.1810 \[gr-qc\]](#).
- [50] V. Gayathri, P. Bacon, A. Pai, E. Chassande-Mottin, F. Salemi, and G. Vedovato, *Phys. Rev. D* **100**, 124022 (2019).
- [51] V. Tiwari *et al.*, *Phys. Rev.* **D93**, 043007 (2016), [arXiv:1511.09240 \[gr-qc\]](#).
- [52] B. J. Owen and B. S. Sathyaprakash, *Phys. Rev.* **D60**, 022002 (1999), [arXiv:gr-qc/9808076 \[gr-qc\]](#).
- [53] L. Vainshtein and V. Zubakov, *Extraction of Signals from Noise: By L.A. Wainstein and V.D. Zubakov* (Dover, 1970).
- [54] T. Dal Canton, S. Bhagwat, S. Dhurandhar, and A. Lundgren, *Class. Quant. Grav.* **31**, 015016 (2014), [arXiv:1304.0008 \[gr-qc\]](#).
- [55] A. H. Nitz, *Class. Quant. Grav.* **35**, 035016 (2018), [arXiv:1709.08974 \[gr-qc\]](#).
- [56] C. Messick *et al.*, *Phys. Rev.* **D95**, 042001 (2017), [arXiv:1604.04324 \[astro-ph.IM\]](#).
- [57] B. Allen, W. G. Anderson, P. R. Brady, D. A. Brown, and J. D. E. Creighton, *Phys. Rev. D* **85**, 122006 (2012).
- [58] G. S. Davies, T. Dent, M. Tpai, I. Harry, C. McIsaac, and A. H. Nitz, (2020), [arXiv:2002.08291 \[astro-ph.HE\]](#).
- [59] S. Babak, R. Biswas, P. R. Brady, D. A. Brown, K. Cannon, C. D. Capano, J. H. Clayton, T. Cokelaer, J. D. E. Creighton, T. Dent, A. Dietz, S. Fairhurst, N. Fotopoulos, G. González, C. Hanna, I. W. Harry, G. Jones, D. Keppel, D. J. A. McKechnan, L. Pekowsky, S. Privitera, C. Robinson, A. C. Rodriguez, B. S. Sathyaprakash, A. S. Sengupta, M. Vallisneri, R. Vaulin, and A. J. Weinstein, *Phys. Rev. D* **87**, 024033 (2013).
- [60] A. H. Nitz, T. Dent, T. Dal Canton, S. Fairhurst, and D. A. Brown, *Astrophys. J.* **849**, 118 (2017), [arXiv:1705.01513 \[gr-qc\]](#).
- [61] T. Dal Canton and I. W. Harry, *arXiv e-prints*, [arXiv:1705.01845 \(2017\)](#), [arXiv:1705.01845 \[gr-qc\]](#).
- [62] T. D. Canton, S. Bhagwat, S. V. Dhurandhar, and A. Lundgren, *Classical and Quantum Gravity* **31**, 015016 (2013).
- [63] A. Bohé *et al.*, *Phys. Rev.* **D95**, 044028 (2017), [arXiv:1611.03703 \[gr-qc\]](#).
- [64] K. Jani, J. Healy, J. A. Clark, L. London, P. Laguna, and D. Shoemaker, *Classical and Quantum Gravity* **33**, 204001 (2016), [arXiv:1605.03204 \[gr-qc\]](#).
- [65] M. Zilhao and F. Löffler, *Proceedings, Spring School on Numerical Relativity and High Energy Physics (NR/HEP2): Lisbon, Portugal, March 11-14, 2013, Int.*

- J. Mod. Phys. **A28**, 1340014 (2013), [arXiv:1305.5299 \[gr-qc\]](#).
- [66] B. P. Abbott *et al.* (LIGO Scientific Collaboration, Virgo Collaboration), [Astrophys. J. Suppl.](#) **227**, 14 (2016), [arXiv:1606.03939 \[astro-ph.HE\]](#).
- [67] B. P. Abbott *et al.* (LIGO Scientific Collaboration, Virgo Collaboration), [Astrophys. J.](#) **833**, L1 (2016), [arXiv:1602.03842 \[astro-ph.HE\]](#).
- [68] R. Biswas, P. R. Brady, J. D. E. Creighton, and S. Fairhurst, [Class. Quant. Grav.](#) **26**, 175009 (2009), [Erratum: [Class. Quant. Grav.](#)30,079502(2013)], [arXiv:0710.0465 \[gr-qc\]](#).
- [69] S. Dhurandhar, A. Gupta, B. Gadre, and S. Bose, [Phys. Rev.](#) **D96**, 103018 (2017), [arXiv:1708.03605 \[gr-qc\]](#).
- [70] B. P. Abbott *et al.* (LIGO Scientific, Virgo), [Phys. Rev.](#) **D96**, 022001 (2017), [arXiv:1704.04628 \[gr-qc\]](#).